
Article:
Baker, J.A., Mouhamad, Y., Hooper, K.E.A. et al. (3 more authors) (2016) From spin coating to roll-to-roll: investigating the challenge of upscaling lead halide perovskite solar cells. IET Renewable Power Generation. ISSN 1752-1416

https://doi.org/10.1049/iet-rpg.2016.0683

From spin coating to roll-to-roll: investigating the challenge of upscaling lead halide perovskite solar cells

J.A. Baker[1], Y. Mouhamad[1,2], K.E.A. Hooper[1], D. Burkitt[1], M. Geoghegan[2], T.M. Watson[1*],
1. SPECIFIC, Swansea University, Bay Campus, Swansea SA1 8EN, UK
2. Department of Physics and Astronomy, The University of Sheffield, Sheffield S3 7RH, UK
* Corresponding Author T.M.Watson@swansea.ac.uk

Abstract

Spin coating, typically used to achieve nanometre thick films, is the established method for depositing perovskite precursors at lab scale for use in solar cells. This paper investigates the dynamics of spin coating perovskite. By combining experimental measurement with a semi-empirical model the evaporation rate of the dimethylformamide (DMF) solvent during the spin coating of a mixed lead halide precursor is determined to be 1.2×10^{-8} m / s. When K-bar coating the same precursor the solvent does not significantly evaporate during the deposition process and when this film is crystallised on a hot plate a rough film results which gives a power conversion efficiency (PCE) of less than 2%. By increasing the airflow of the K-bar coated perovskite film during crystallisation to 2.7×10^{-4} m / s the PCE increases significantly to 8.5% through an improvement in short circuit current and fill factor.

1. Introduction

There are a number of photovoltaic technologies such as organic photovoltaics [1], dye sensitised solar cells [2,3] and perovskite cells [4,5], which aim to capitalise on the lower fabrication costs of roll-to-roll solution processing. Since 2012 perovskite solar cells have become the most efficient of the solution processed photovoltaic (PV) technologies [6,7] with small-scale devices reporting a power conversion efficiency (PCE) in excess of 20% [8,9]. Spin coating is often favoured as a convenient method to deposit solution processed solar cells when large areas are not needed. Spin coating is limited in commercial production by a high percentage of material wastage, the difficulty of batch processing and constraints on substrate size (typically < 100 cm^2).

In order for perovskite solar cells to realise their potential as a low cost PV technology, deposition methods suitable for large area production need to be developed. One of the most challenging layers to deposit by processes compatible with large scale production is the active lead halide perovskite layer itself since this usually requires *in situ* formation of the perovskite material from two precursor materials; methyl ammonium (MA) iodide and lead halide.

Mixed halide perovskites are formed by a reaction between methyl ammonium halide and lead halide (Eqn 1). In this example, the precursor of MAI and lead (II) chloride ($PbCl_2$) in a polar solvent is co-deposited onto the substrate and spin coated. Typically a heating step at 100ºC ensures complete conversion into perovskite.

$$3\,MAI + PbCl_2 \rightarrow MAPbI + 2\,MACl \quad (1)$$

By spin coating the precursor, substantial solvent can be removed at room temperature prior to the annealing step [10] whereby the perovskite film is formed. Spinning toluene onto the spin coated film prior to annealing has been shown to improve the quality of the film further [11].

Roll-to-roll compatible techniques such as slot die coating [12-14], blade coating [15,16] and K-bar coating [17,18], can also be used to deposit the precursor. Slot-die coating deposits the solution directly onto the substrate through a precisely machined die, under which the substrate passes underneath, as shown in Fig. 1a. The solution is metered by controlling the substrate speed and the pump speed of the solution through the die. K-bar coating is also a direct deposition technique where the solution is deposited by a wire-wound bar that moves across the substrate, as shown in Fig. 1b-c. The solution is metered by changing the diameter of the wires wound around the bar.

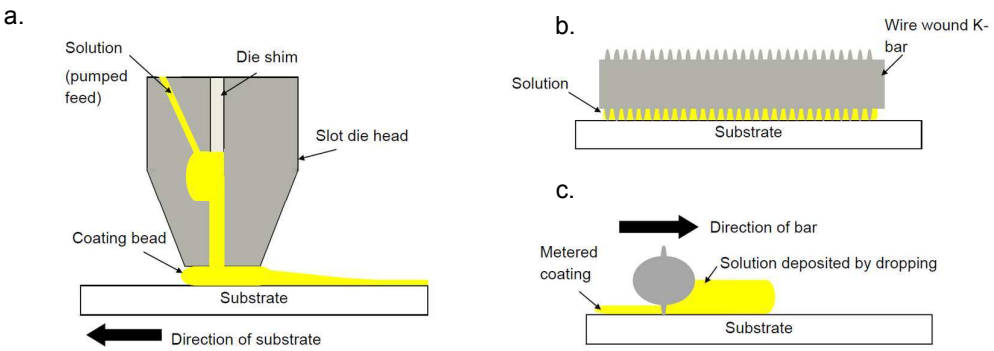

Figure 1 Schematic diagram showing (a) slot-die coating, side view. (b) K-bar coating, front view, (c) K-bar coating side view

Both slot die and K-bar coating involve the direct deposition of the precursor onto the substrate and therefore these techniques use much less material overall than spin coating (5 ml m^{-2} rather than 240 ml m^{-2}).

The disadvantage of the direct deposition is that there is no dynamic drying before the deposition step and this can make it very difficult to control the crystallisation process. To date the highest performing devices have been produced by spin coating [19]. The composition of the spin coated solution, the spin speed, the initial acceleration, the spin duration were shown to be essential for the grain size of the crystals [21]. These parameters also govern the rate at which the films thin as reported by the Meyerhofer [22] equation,

$$\frac{dh}{dt} = -\frac{2\omega^2}{3\eta} - e \quad . \qquad (2)$$

Here *h* is the film thickness, ω the spin speed, η the viscosity and *e* a constant evaporation rate. The first term on the right of Eqn 2 is the vertical velocity of the film. In other words the magnitude at which the film reduces in thickness is equal to the axial velocity plus the evaporation rate. Solvent evaporation is controlled by two phenomena: the diffusion of the solvent molecules in the film and the solvent partial pressure above the film.

Despite the proven effectiveness of spin coating to deposit the lead halide perovskite layer the dynamics of this process has not been investigated. Understanding the dynamics of spin coating is key to develop a processing method which will enable the scale-up of perovskite cells. This paper examines the dynamics of spin coating perovskite precursor materials in order to understand the key parameters governing film formation during spin coating. An initial study into the effect of airflow on the performance of K-bar coated perovskite devices is undertaken.

2. Experimental

2.1 Film deposition and characterisation

Perovskite films were prepared on 7 Ω / □ conductive fluorine-doped tin oxide (FTO) glass, cleaned with 2% Hellmanex in deionised water, rinsed with deionised water and then oxygen plasma treated. A compact TiO_2 layer (50 nm) was deposited via spray pyrolysis at 300°C from a solution 1:10 of titanium di-isopropoxide bis(acetylacetonate) and isopropanol before undergoing a sintering step at 550°C (30 min). A 40 wt% precursor solution of MAI and $PbCl_2$ (3:1 molar ratio) in DMF was prepared in a nitrogen atmosphere and used for the spin coating and K-bar coating trials, which were both carried out in laboratory conditions. The spin-coated films were prepared by dropping 150 µl of perovskite precursor solution onto the substrate (25 mm^2) and spinning at 2000 rpm for 45 s before heating on a hot plate at 100ºC. The K-bar samples were prepared by coating 50 µl of perovskite precursor solution at a speed of 0.6 m / min onto a substrate (100 mm x 200 mm) and heating on a hot plate for 1 h at 100ºC or by a forced air oven with an air flow of 2.7 x 10^{-4} m/s (1000 l / m^2 / h). Surface roughness measurements were taken using a DEKTAK profilometer over a distance of 1 mm and with a resolution of 330 nm.

2.2 Solar cell fabrication and characterisation

To fabricate solar cells a compact TiO_2 layer (50 nm) was deposited onto laser etched FTO via spray pyrolysis as detailed in section 2.1. Then a mesoporous TiO_2 film was deposited and sintered at 550ºC. The perovskite film was deposited by either spin coating or bar coating as described in section 2.1. A 10 wt% solution containing 2,2′,7,7′-tetrakis-(*N*,*N*-di-*p*-

methoxyphenyl-amine)-9,9′-spirobifluorene (Spiro-OMeTAD) in chlorobenzene, doped with 4-*tert*-butylpyridine and lithium bis-trifluoromethane sulfonimide, was spin coated over the spin coated perovskite layer at 2000 rpm to form the hole transport layer (HTL). For the K-bar coated devices poly(3-hexylthiophene-2,5-diyl) Mr 15000 – 45,000 in chlorobenzene (15 mg / ml) K-bar coated at a speed of 0.6 m / min, was used as the HTL Gold contacts were been thermally evaporated onto the HTL to complete the device stack. I-V testing was performed using an Oriel solar simulator with a KG5 filter, at 1 sun AM1.5 and a Keithley 2400 source meter. The cells had 10 s of light soaking before each measurement and were scanned at a rate of 0.15 V / s from 1.1 V to –0.1 V. The active area of solar cells was defined through a metal aperture mask with an open area of 0.09 cm^2.

2.3 Optospinometery

In situ light scattering of the spin coating process (optospinometry, Fig. 2) was performed using a 633 nm laser focused onto a chuck rotating at 2000 rpm. The angle between the laser and the photo diode was 45º. The refractive index of the perovskite precursor was measured as 1.4 by refractometry. The viscosity of the perovskite precursor was measured using a Bohlin Rheometer, with a 55 mm diameter cone and plate, the cone angle was 2°.

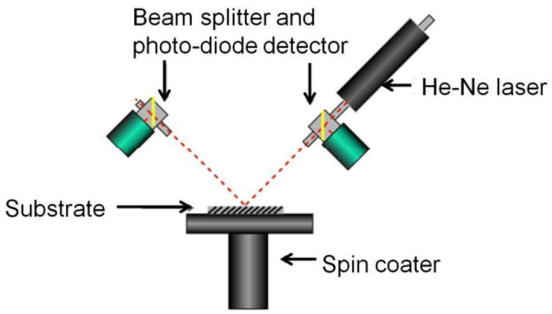

Figure 2 Set-up of the optospinometer.

3. Results and Discussion

In order to fully understand the extent of dynamic drying during spin coating, optospinometry was performed. Fig. 3a shows the reflectivity of the perovskite precursor during spin coating.

The peaks are obtained when light reflected by the top and bottom of the film is in phase i.e. Bragg's law is satisfied. The destructive interference is caused when this is out of phase.

The change in film thickness (Δh) was obtained from the distance between interference peaks,

$$\Delta h = \frac{\lambda}{2n\sin\theta} \quad (2)$$

where n is the refractive index, θ the incident angle and λ is the laser wavelength. Knowing the final thickness of the film, the change in thickness can be calculated as shown in Fig. 3b. In previous work it was shown [23] was shown that the Meyerhofer equation does not account for the inertial forces which are important in the early stage of the process. A semi-empirical model was used to model the thinning of the film [23] shown in Fig. 3b by

$$\frac{dh}{dt} = -\frac{2\omega^2}{3\eta} - \frac{B}{\exp\left(U\frac{t}{\tau}\right)} - e, \quad (3)$$

where B and U are fitting parameters which are functions of viscosity (η) but independent of h. Here τ = 1 s. B represents initial resistance to the thinning of the film due to the presence of the inertial force and B / exp(Ut/ τ) represents the rate at which the resistance decreases. The axial velocity of the fluid is expressed by

$$v_r = -\frac{2\omega^2}{3\eta} - \frac{B}{\exp\left(U\frac{t}{\tau}\right)}. \quad (4)$$

The axial velocity was plotted (Fig. 3c) by replacing the fitting parameters in Eqn 4. Spin coating is a two-stage process; initially the film thickness is governed by the viscous forces. In the second stage the film is too dense to flow and the evaporation of solvent dominates the process. This is clearly illustrated in Fig. 3c, where the axial velocity of the film decreases rapidly and becomes negligible after 10 s. The model gives an evaporation rate equal to 1.2 x

10^{-8} m/s, demonstrating that following initial film thinning due to radial material displacement there is significant evaporation of the solvent.

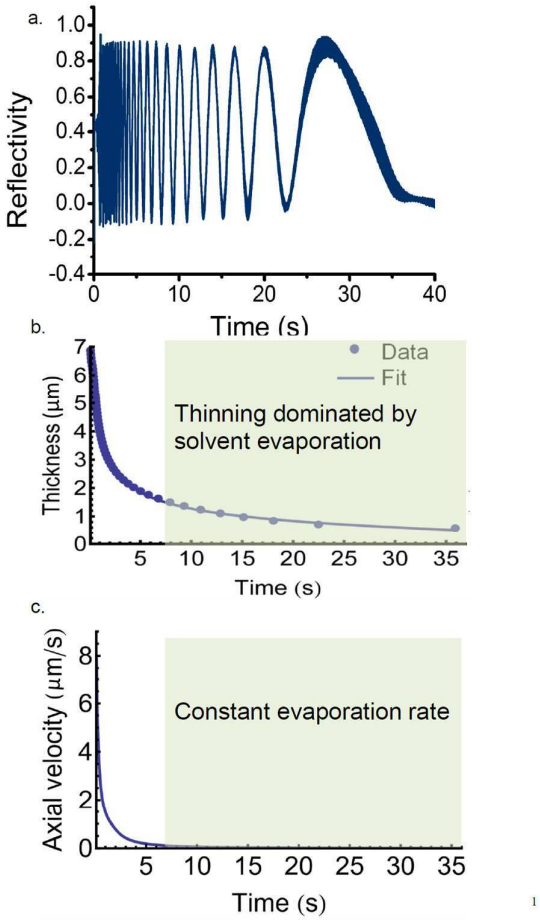

Figure 3 (a) Specular reflectivity during the spin coating of perovskite precursor. (b) Comparison of modelled and experimental data showing the thickness of the drying film as a function of time during spin coating. (c) Modelled axial velocity as a function of time

After 45 s of spinning, an intermediate phase of transparent crystals has already formed, Fig. 4a. After K-bar coating a liquid film remains (not shown) on the substrate until the start of the annealing. In order to confirm whether the fast solvent evaporation during spin coating controls the quality of the film, we studied the morphology of K-bar coated films annealed under different conditions. Solvent evaporation is driven by two phenomena: the diffusion of

the solvent molecules in the film and the solvent partial pressure above the film. Annealing of the spin coated perovskite film, required for perovskite formation and crystal growth, leads to a film with rounded perovskite crystals; Fig. 4b, a film thickness of ~ 200 nm and a roughness (R_a) of 150 nm. Further advances in the spin-coating process which use the toluene drip method [11] in order to remove further the solvent have been shown to create much smoother films but these are outside the scope of this work.

By comparison, films coated using the K-bar method and using standard hot plate annealing have crystals which grow vertically and a dendritic type structure is produced as shown in Fig. 4c, with an average thickness of 1.2 μm and an R_a of 920 nm.

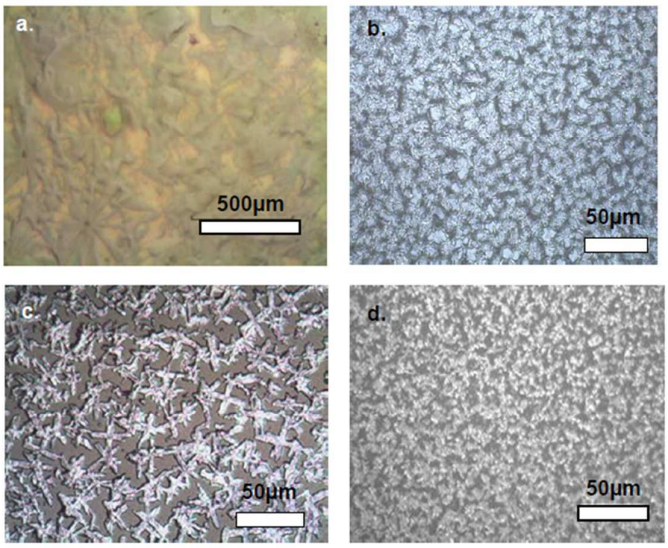

Figure 4 Optical microscopy images of (a) Perovskite precursor film after spin coating. (b) Spin coated perovskite film after hot plate annealing. (c) K-bar coated perovskite film after hot plate annealing (d) K-bar coated perovskite film annealed in a forced air oven 1000 l / m^2 /h

By heating the K-bar coated film in a forced-air oven (instead of using a hot plate) with a flow rate of 1000 l / m^2 / h (equivalent to 2.7 x 10^{-4} m / s) the solvent evaporation was increased since the air above the film is not saturated with solvent. Fig. 4d shows that films dried in a forced-air oven have an appearance more similar to the spin coated sample and with a film thickness of 420 nm and an R_a of 310 nm.

In order to investigate whether dewetting also has an influence on the film formation, the contact angle of the perovskite precursor on different substrates was measured. The contact angle of the perovskite precursor with the TiO_2 coated FTO glass is less than 25°, indicating good wetting, as shown in Fig. 5.

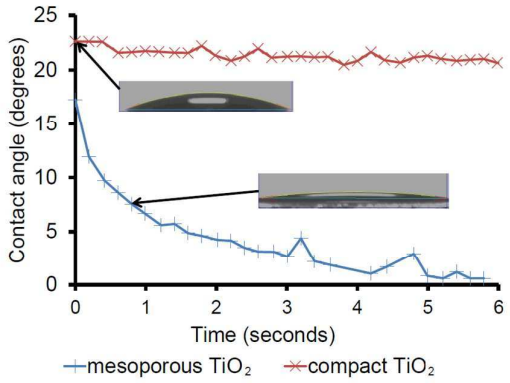

Figure 5 Comparison of contact angle of perovskite precursor on mesoporous and compact TiO_2 films. Inserts are photographs of contact angle measurement, the drop size is 4 μl. The lower image shows a reduction in contact angle signifying better surface wetting.

When a mesoporous TiO_2 scaffold is used complete wetting is achieved within 5 s as the perovskite precursor infiltrates the porous TiO_2. This implies that whilst substrate choice can affect the film wetting it is not a primary cause of rough perovskite crystal morphology. This supports previous findings where slot-die coated perovskite films deposited on glass and TiO_2 mesoporous scaffold have very similar morphologies when annealed under similar conditions [14].

To confirm the effect of annealing air flow rate on device performance perovskite films processed using the same conditions as the films in Fig 4b-c were manufactured into solar cell devices, i.e. spin coated annealed with a hot plate, K-bar coated annealed with a hot plate and K-bar coated annealed in a forced air oven with a flow rate of 1000 l / m^2 / h. The device performances of these cells are compared in Fig. 6.

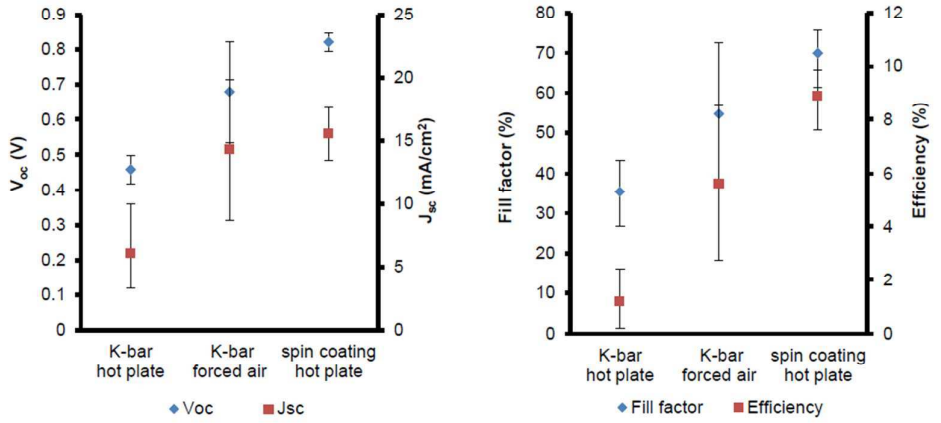

Figure 6 (a) Comparison of perovskite processing conditions on short-circuit current (J_{sc}) and open-circuit voltage (V_{oc}) of perovskite solar cell devices. (b) Comparison of perovskite processing condition on fill factor and PCE of perovskite solar cell devices. Error bars indicate the standard deviation of eight identical devices

The hot plate annealed K-bar coated cells have low J_{sc} attributed to poor perovskite coverage and a low V_{oc} also attributed to poor coverage causing shunting between the HTM and the TiO_2. The best K-bar coated cell with forced air annealing had similar characteristics to the spin-coated samples with a PCE of 8.5% (compared with the spin coated hot plate device with a PCE of 9.9%). Across the batch the current density of the forced air devices is more variable than for the spin coated devices indicating that the conversion process is not as controlled as for the spin coated device. Further work is needed to improve the uniformity of the perovskite film formation, focussing on high air flow in-line solutions as well as in-line compatible anti-solvent methods.

4. Conclusions

The high efficiencies of perovskite cells mean they have great promise as a low cost PV technology. By studying the dynamics of spin coating it has been demonstrated that fast solvent evaporation is a key parameter in the formation of the perovskite film. It has also been shown that better coverage and improved cell performance can be obtained with K-bar coated

by increasing the solvent evaporation rate using a forced air oven, increasing the maximum PCE from 2.4% to 8.5%. Whilst this improvement is significant further improvements are needed to improve the consistency of the devices and to match the performance of the best spin coated devices.

5. Acknowledgments

This work was part-funded by EPSRC Supersolar, EP/J017361/1 (JB). EP/E04591X/01 (YM/MG). The authors would like to thank the EPSRC and TSB for supporting this work through the SPECIFIC Innovation and Knowledge Centre EP/N020863/1.

6. References

[1] F. C. Krebs, “Fabrication and processing of polymer solar cells: A review of printing and coating techniques,” Solar Energy Materials and Solar Cells, 93, no. 4, pp. 394–412, 2009.

[2] B. O’Regan and M. Grätzel, “A low-cost, high-efficiency solar cell based on dye-sensitized colloidal TiO_2 films,” Nature, 353, pp. 737–740, 1991.

[3] J. Baker, D. Deganello, D. T. Gethin, et al., “Flexographic printing of graphene nanoplatelet ink to replace platinum as counter electrode catalyst in flexible dye sensitised solar cell,” Materials Research Innovations, 18, no. 2, pp. 86–90, 2014.

[5] H. J. Snaith, “Perovskites : The Emergence of a New Era for Low-Cost, High-Efficiency Solar Cells,” J. Phys. Chem. Lett, 4, p. 3623−3630, 2013.

[6] M. M. Lee, J. Teuscher, T. Miyasaka, et al., “Efficient Hybrid Solar Cells Based on Meso-Superstructured Organometal Halide Perovskites,” Science, 338, no. 6107, pp. 643–647, 2012.

[7] H.-S. Kim, C.-R. Lee, J.-H. Im, et al., “Lead Iodide Perovskite Sensitized All-Solid-State Submicron Thin Film Mesoscopic Solar Cell with Efficiency Exceeding 9%,” Scientific Reports. 2, 591, pp. 1–7, 2012.

[8] W. S. Yang, J. H. Noh, N. J. Jeon, et al., “High-performance photovoltaic perovskite layers fabricated through intramolecular exchange,” Science, vol. 348, Issue 6240, pp. 1234-1237, 2015

[9] X. Li, D. Bi, C. Yi, et al., “A vacuum flash-assisted solution process for high-efficiency large-area perovskite solar cells,” Science, vol. 8060, no. June, pp. 1–10, 2016.

[10] R. Kang, J.-E. Kim, J.-S. Yeo, et al., “Optimized Organometal Halide Perovskite Planar Hybrid Solar Cells via Control of Solvent Evaporation Rate,” The Journal of Physical Chemistry C, vol. 118 (46), pp 26513–26520 2014.

[11] N. J. Jeon, J. H. Noh, Y. C. Kim, et al.,“Solvent engineering for high-performance inorganic-organic hybrid perovskite solar cells.,” Nature materials, vol. 13, pp 897–903, 2014.

[12] K. Hwang, Y. S. Jung, Y. J. Heo, et al., "Toward large scale roll-to-roll production of fully printed perovskite solar cells," Advanced Materials, vol. 27, no. 7, pp. 1241–1247, 2015.

[13] D. Vak, K. Hwang, A. Faulks, et al., "3D Printer Based Slot-Die Coater as a Lab-to-Fab Translation Tool for Solution-Processed Solar Cells," Advanced Energy Materials, vol. 5, no. 4, 2015.

[14] G. Cotella, Baker J., De Rossi F, et al., "One-step deposition by slot-die coating of mixed lead halide perovskite for photovoltaic applications," Solar Energy Materials and Solar Cells, 159, pp 362-369, 2017.

[15] S. Razza, F. Di Giacomo, F. Matteocci, et al., "Perovskite solar cells and large area modules (100 cm^2) based on an air flow-assisted PbI_2 blade coating deposition process," Journal of Power Sources, vol. 277, no. 2015, pp. 286–291, 2015.

[16] F. Di Giacomo, S. Razza, F. Matteocci, et al., "High efficiency $CH_3NH_3PbI_{(3-x)}Cl_x$ perovskite solar cells with poly(3-hexylthiophene) hole transport layer," Journal of Power Sources, vol. 251, pp. 152–156, 2014.

[17] K. E. A. Hooper, B. Smith, P. Greenwood, et al., "Spray PEDOT:PSS Coated Perovskite with a Transparent Conducting Electrode for Low Cost Scalable photovoltaic Devices," Materials Research Innovations, no. 7, pp. 482–487, 2015.

[18] E. W. Jones, P. J. Holliman, A. Connell, et al., "A novel dimethylformamide (DMF) free bar-cast method to deposit organolead perovskite thin films with improved stability," Chem. Commun., vol. 52, pp. 4301–4304, 2016.

[19] X. Li, D. Bi, C. Yi, et al., "A vacuum flash–assisted solution process for high-efficiency large-area perovskite solar cells," Science, vol. 860 Jun. 2016.

[20] W. Qiu, T. Merckx, M. Jaysankar, et al., "Pinhole-Free Perovskite Films for Efficient Solar Modules," Energy & Environmental Science, vol. 9, pp. 484-489, 2016.

[21] W. Nie, H. Tsai, R. Asadpour, et al.,"High-efficiency solution-processed perovskite solar cells with millimeter-scale grains," Science , vol. 347 , no. 6221 , pp. 522–525, 2015.

[22] D. Meyerhofer, "Characteristics of resist films produced by spinning" J. Appl. Phys. vol. 49, 3993,1978.

[23] Y. Mouhamad, P. Mokarian-Tabari, N. Clarke, et al., "Dynamics of polymer film formation during spin coating," Journal of Applied Physics, vol. 116, no. 12, p. 123513, 2014.

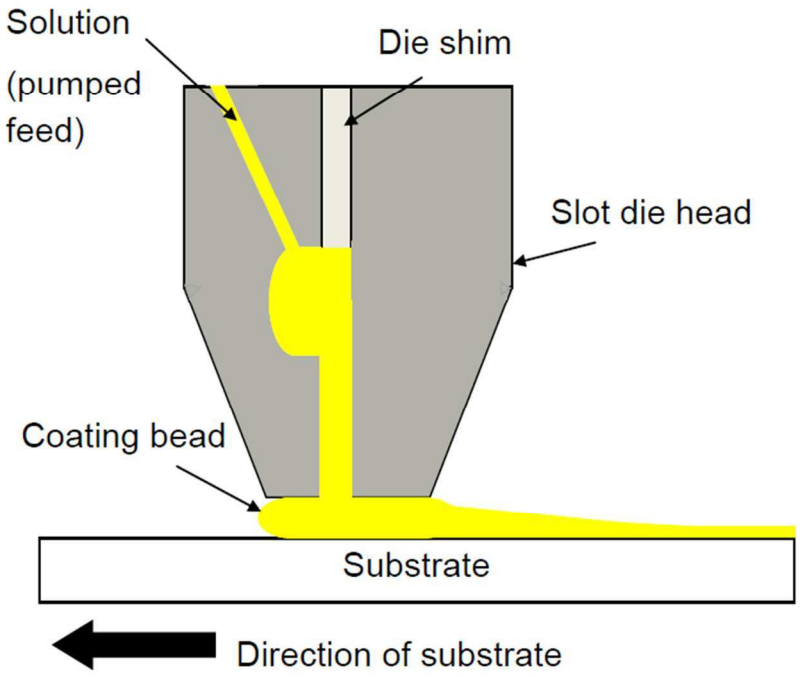

Figure 1 Schematic diagram showing (a) slot die coating, side view. (b) K-bar coating, front view, (c) K-bar coating side view.

Fig. 1a
225x165mm (96 x 96 DPI)

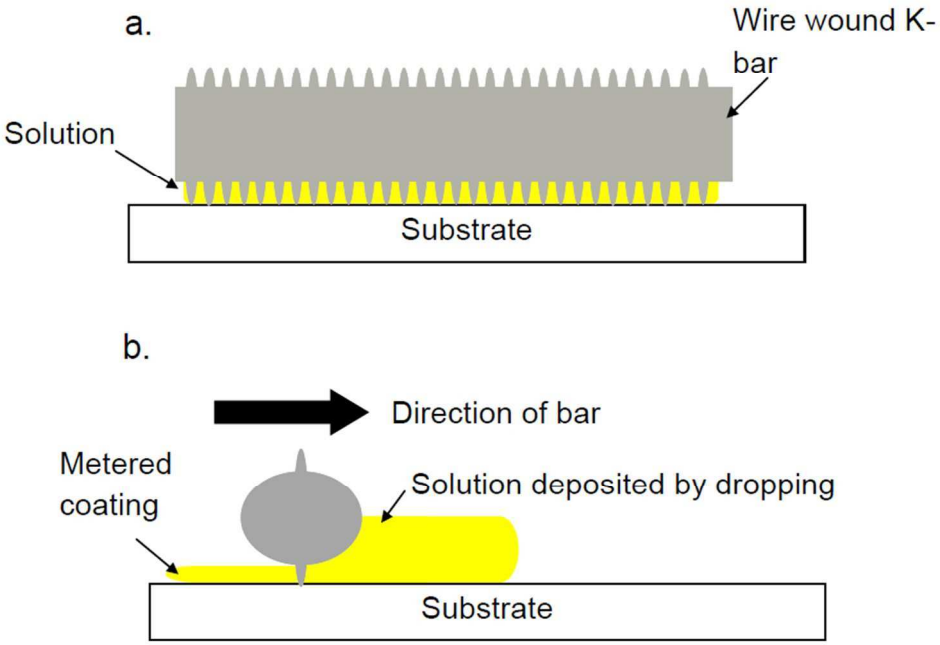

Figure 1 Schematic diagram showing (a) slot die coating, side view. (b) K-bar coating, front view, (c) K-bar coating side view.
Fig. 1b-c
251x182mm (96 x 96 DPI)

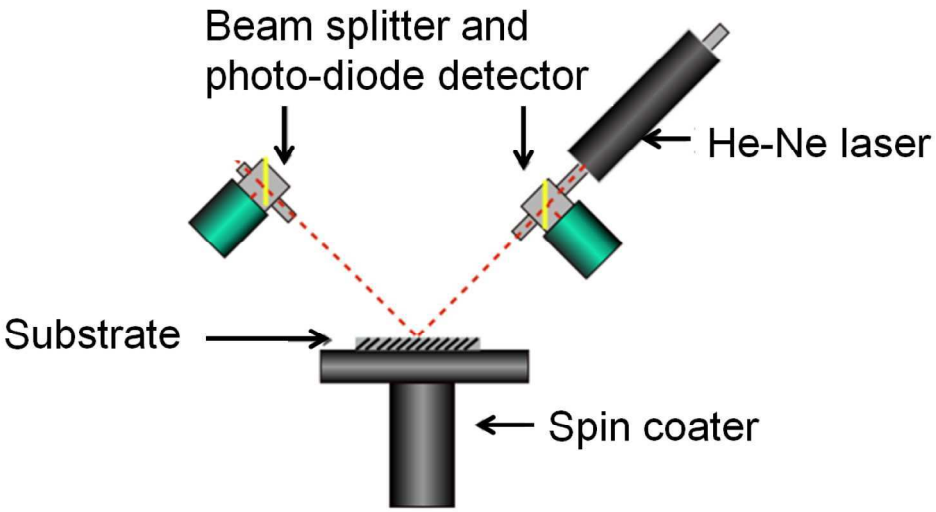

Figure 2 Set-up of the optospinometer.
Fig. 2
219x120mm (300 x 300 DPI)

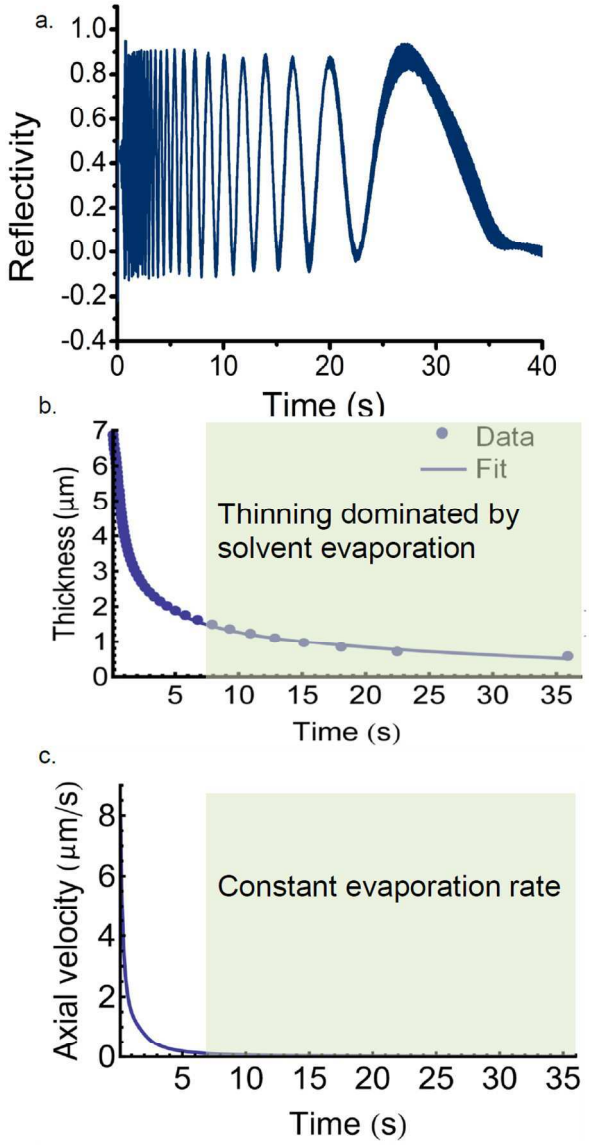

Figure 3 (a) Specular reflectivity during the spin coating of perovskite precursor. (b) Comparison of modelled and experimental data showing the thickness of the drying film as a function of time during spin coating. (c) Modelled axial velocity as a function of time

Fig. 3a
293x473mm (96 x 96 DPI)

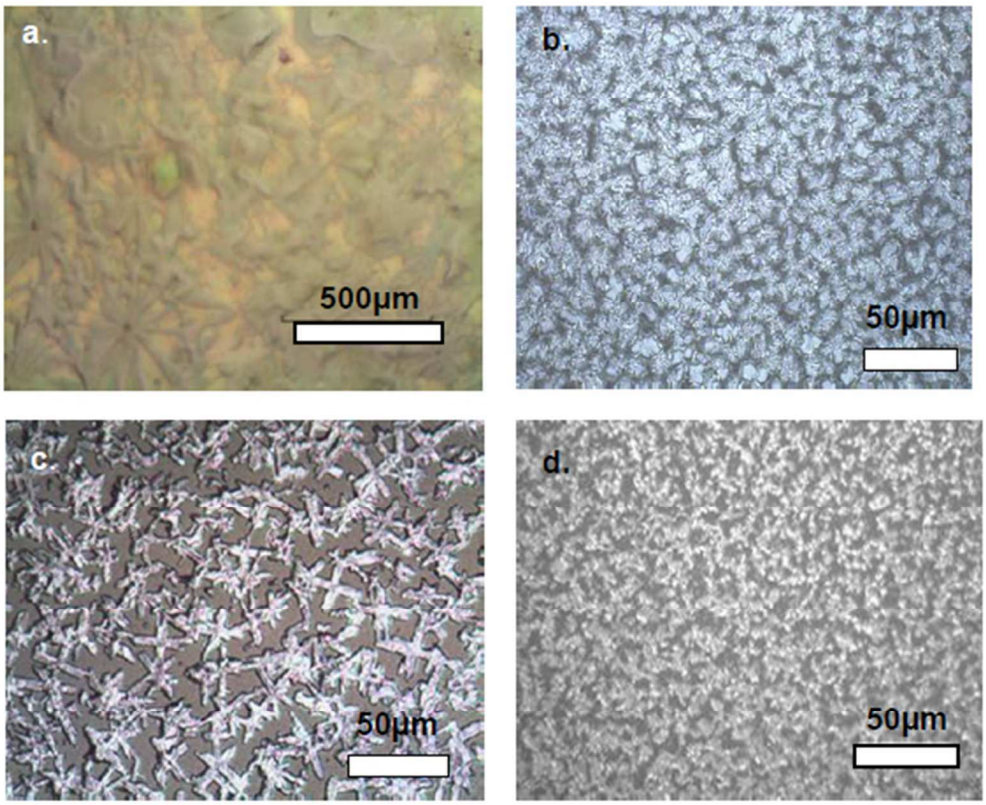

Figure 4(a) Perovskite precursor film after spin coating. (b) Spin coated perovskite film after hot plate annealing. (c) K-bar coated perovskite film after hot plate annealing (d) K-bar coated perovskite film annealed in a forced air oven 1000 l / m2 /h

Fig. 4a
151x123mm (96 x 96 DPI)

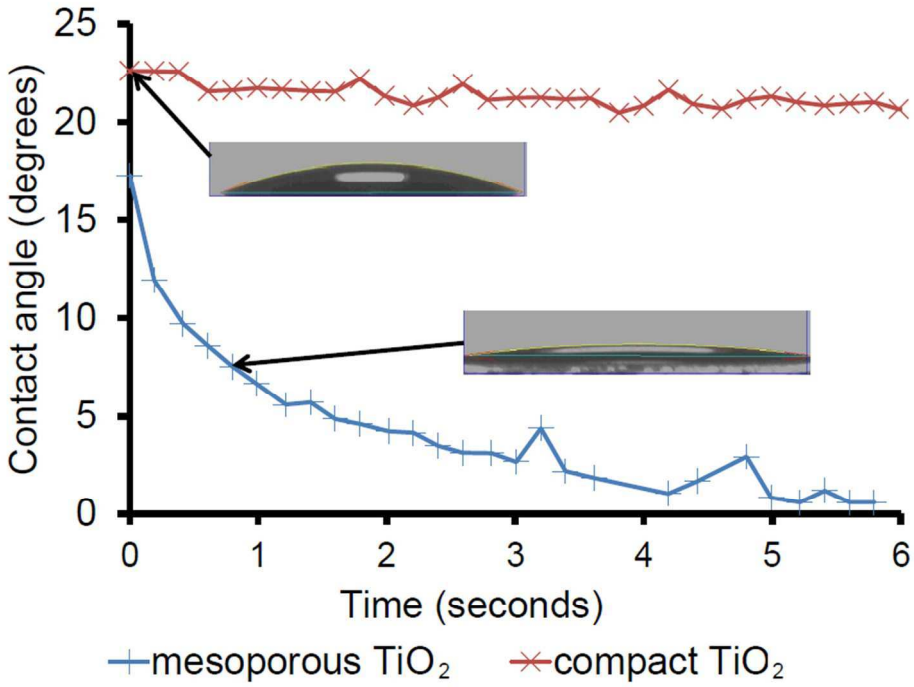

Figure 5 Comparison of contact angle of perovskite precursor on mesoporous and compact TiO2 films.
Fig. 5
254x187mm (96 x 96 DPI)

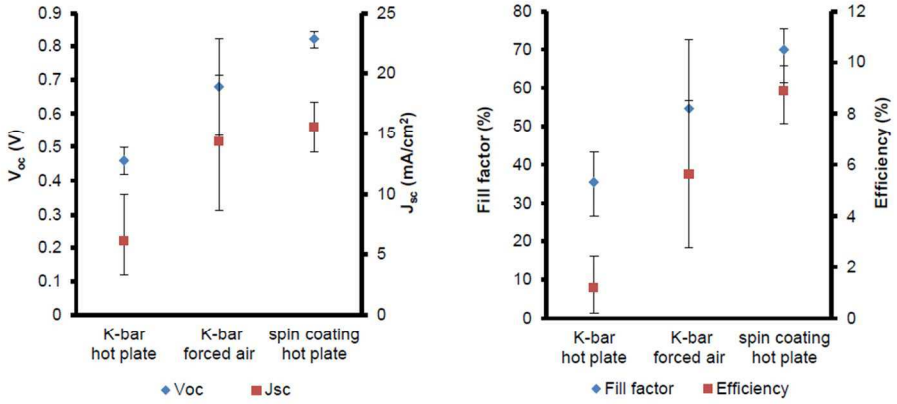

Figure 6(a) – Comparison of perovskite processing conditions on short circuit current (Jsc) and open circuit voltage (Voc) of perovskite solar cell devices. (b) Comparison of perovskite processing condition on fill factor and PCE of perovskite solar cell devices. Error bars indicate standard deviation of eight identical devices

Fig. 6
284x141mm (96 x 96 DPI)